Centrum voor Wiskunde en Informatica
Centre for Mathematics and Computer Science

B. Koren

Euler flow solutions for a transonic windtunnel section

Department of Numerical Mathematics Report NM-R8601 January

The Centre for Mathematics and Computer Science is a research institute of the Stichting Mathematisch Centrum, which was founded on February 11, 1946, as a nonprofit institution aiming at the promotion of mathematics, computer science, and their applications. It is sponsored by the Dutch Government through the Netherlands Organization for the Advancement of Pure Research (Z.W.O.).

Euler Flow Solutions for a Transonic Windtunnel Section

B. Koren
Centre for Mathematics and Computer Science
P.O. Box 4079, 1009 AB Amsterdam, The Netherlands

2-D Euler flow computations have been performed for a windtunnel section, designed for research on transonic shock-wave boundary-layer interaction. For the discretization of the Euler equations, a finite volume Osher discretization has been applied. The solution method is a non-linear multigrid iteration with symmetric point Gauss-Seidel as a relaxation method. Initial finest grid solutions have been obtained by full multigrid. Some grid adaptation has been applied for obtaining a sharp shock. An indication is given of the mathematical quality of 4 different boundary conditions for the outlet flow. The solutions of two transonic flows with shock are presented; a choked and a non-choked flow. Both flow solutions show a good shock capturing.

1980 Mathematics Subject Classification: 35B30, 65N50, 76G15, 76H05.
Key Words and Phrases: steady Euler equations, transonic flows, grid generation and adaptation, boundary conditions.
Note: This report will be submitted for publication elsewhere.

1. Introduction

An important physical feature for the design of transonic airfoils is the interaction between the possible shock wave(s) at the airfoil and the thin viscous layer (boundary layer) around the airfoil. In transonic aerodynamics a lot of work, both experimental and theoretical, is devoted to this so-called transonic shock-wave boundary-layer interaction. At the Delft University of Technology a transonic windtunnel section has been designed and constructed for performing measurements on this phenomenon [1]. Limited accessibility to the flow in the windtunnel section inhibits measurements throughout the entire flow field. However, knowledge of the entire flow field is important for redesign purposes. This situation motivated a computation of the entire flow field.

As a suitable computational approach has been chosen: to determine and match, in an iterative way, the solutions of the steady 2-D Euler and boundary layer equations. The solutions of the Euler equations are the topic of this report.

Of main importance for an Euler flow computation, supporting measurements on transonic shock-wave boundary-layer interaction, is a good resolution of the shock wave. Well-suited for this purpose is the method developed by Hemker and Spekreijse [2]. The method uses a finite volume Osher discretization, yielding solutions with shocks satisfying all commonly required conditions (monotonicity, sharp shocks, conservation of mass, momentum and energy, and agreement with the entropy condition).

2. Computational Method

Hemker and Spekreijse developed a solution method in which they discretized the steady 2-D Euler equations, defined on the domain Ω by

$$\frac{\partial f(q)}{\partial x} + \frac{\partial g(q)}{\partial y} = 0, \text{ with} \tag{2.1}$$

$$q = \begin{bmatrix} \rho \\ \rho u \\ \rho v \\ \rho e \end{bmatrix}, \quad f = \begin{bmatrix} \rho u \\ \rho u^2 + p \\ \rho uv \\ \rho u(e + \frac{p}{\rho}) \end{bmatrix}, \quad g = \begin{bmatrix} \rho v \\ \rho vu \\ \rho v^2 + p \\ \rho v(e + \frac{p}{\rho}) \end{bmatrix}, \text{ and} \tag{2.2}$$

$$e = \frac{1}{\gamma - 1}\frac{p}{\rho} + \tfrac{1}{2}(u^2 + v^2), \tag{2.3}$$

in their integral form

$$\int_{\delta\Omega} (f n_x + g n_y) ds = 0. \tag{2.4}$$

In (2.2) and (2.3) ρ, u, v, p and γ denote respectively: density, velocity components in x- and y-direction, static pressure and ratio of specific heats. In (2.4) $\delta\Omega$ denotes the boundary of an arbitrary subregion of the domain Ω, and n_x and n_y denote the components of the outward normal along $\delta\Omega$.

A simple way to discretize (2.4) is to subdivide Ω into disjoint quadrilateral subregions Ω_{ij} (finite volumes). This yields the discretized form

$$\sum_{k=1}^{4} \int_{\delta\Omega_{ij,k}} (f_{ij,k} n_{x_{ij,k}} + g_{ij,k} n_{y_{ij,k}}) ds = 0, \quad \text{for all } ij, \tag{2.5}$$

in which the subscript k refers to the four sides of the quadrilateral Ω_{ij}.

Assuming the solution to be constant in each volume, and taking $f_{ij,k}$ and $g_{ij,k}$ as functions of the states in the neighbouring volumes Ω_{ij} and $\Omega_{ij,k}$ only, (2.5) simplifies to the first order accurate discretization

$$\sum_{k=1}^{4} \{f(q_{ij}, q_{ij,k}) n_{x_{ij,k}} + g(q_{ij}, q_{ij,k}) n_{y_{ij,k}}\} s_{ij,k} = 0, \quad \text{for all } ij, \tag{2.6}$$

with $s_{ij,k}$ the length of side k of volume Ω_{ij}.

For the Euler equations, because of their rotational invariance, (2.6) may be further simplified to

$$\sum_{k=1}^{4} T_{ij,k}^{-1} f(T_{ij,k} q_{ij}, T_{ij,k} q_{ij,k}) s_{ij,k} = 0, \quad \text{for all } ij, \text{ with} \tag{2.7}$$

$$T_{ij,k} = \begin{bmatrix} 1 & 0 & 0 & 0 \\ 0 & n_{x_{ij,k}} & n_{y_{ij,k}} & 0 \\ 0 & -n_{y_{ij,k}} & n_{x_{ij,k}} & 0 \\ 0 & 0 & 0 & 1 \end{bmatrix}. \tag{2.8}$$

Given this discretization, the problem is to evaluate the vector function f at the volume walls. A way to evaluate f is to consider the flow at each volume wall as the local solution at $t = t_0 + \Delta t$ for $\Delta t \to 0$, of the 1-D Riemann problem of two gas states (q_{ij} and $q_{ij,k}$) initially meeting as a discontinuity. The exact solution of the Riemann problem yields the Godunov scheme for discretization. A disadvantage of the Godunov scheme are its high costs. Several more economical, so-called approximate Riemann solvers exist. Hemker and Spekreijse have chosen the approximate Riemann solver proposed by Osher [3]. Their motives were: (1.) its consistent treatment of boundary conditions, and particularly (2.) its convenience for Newton-type solution techniques for (2.7). The Osher scheme, known to be more elaborate than other approximate Riemann solvers, has been implemented in the relatively simple way as proposed by Hemker and Spekreijse (their so-called *P*-variant).

To solve the non-linear system (2.7), Hemker and Spekreijse considered point relaxation methods, in which they used a local Newton iteration for the collective relaxation of the 4 unknowns in each single volume. These relaxation methods are simple and robust, but need an acceleration. When using symmetric point Gauss-Seidel as a relaxation method (as has been done here), a suitable acceleration technique is found in multigrid. As an efficient and robust multigrid technique Hemker and Spekreijse found: multigrid in its non-linear form (FAS), preceded by full multigrid (FMG). By using FMG they bypassed the danger of using an initial finest grid solution outside the convergence range. This multigrid technique has been adopted as well for the present computations

3. Grid Generation and Adaptation

In order to obtain a good resolution of large local gradients (which are decided to be of practical importance), and yet not to have high computational costs, one should use grids with local refinements. In order not to lose the order of accuracy of the computational method, the refinements should be sufficiently smooth in all grids used in the multigrid process.

For the computational results shown in the remainder of this paper we used grids with stretching, as shown (for a 4-level multigrid strategy) in figure 3.1.

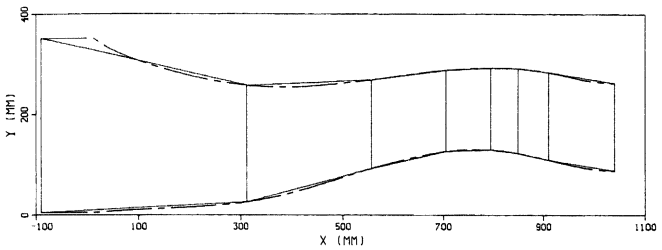

FIGURE 3.1a 7×1-grid.

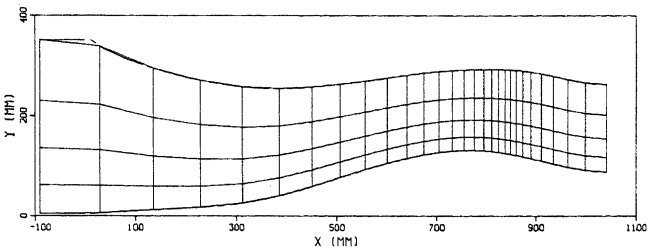

FIGURE 3.1c 28×4-grid.

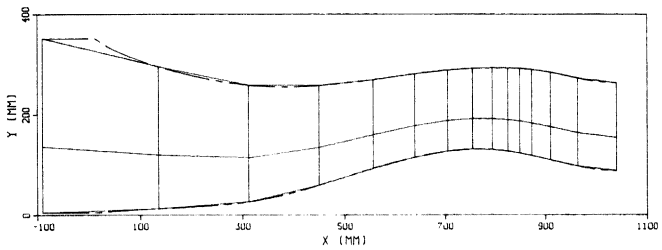

FIGURE 3.1b 14×2-grid.

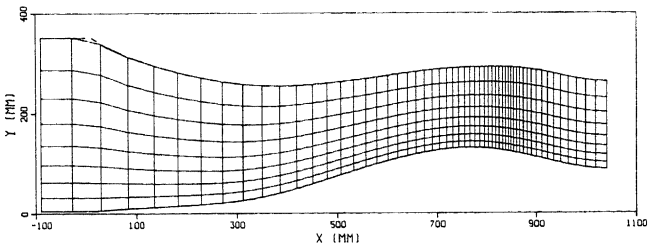

FIGURE 3.1d 56×8-grid.

The dashed lines indicate the lower and upper wall. The modest grid refinement from upper to lower wall has been introduced to give more detail to gradients in y-direction in especially the shock region.

At first it has also been tried to obtain a good resolution of the expected gradients at the kink in the upper wall, by using for all grids in the multigrid strategy a vertical grid line at the kink and by using a local refinement at this location as well. Independent of the rate of refinement at the kink, the solutions showed the same defect ($p > p_{t_{inlet}}$) in this particular region. This suggested that the method had lost its first order accuracy at this location. A small investigation, using a family of equidistant grids, proved that this was the case indeed (figure 3.2a, with the markers indicating the x-locations of the centres of the volume walls). The reason for the loss of first order accuracy is the lack of grid smoothness at the kink, as shown by a computation with a smoothed upper wall (figure 3.2b).

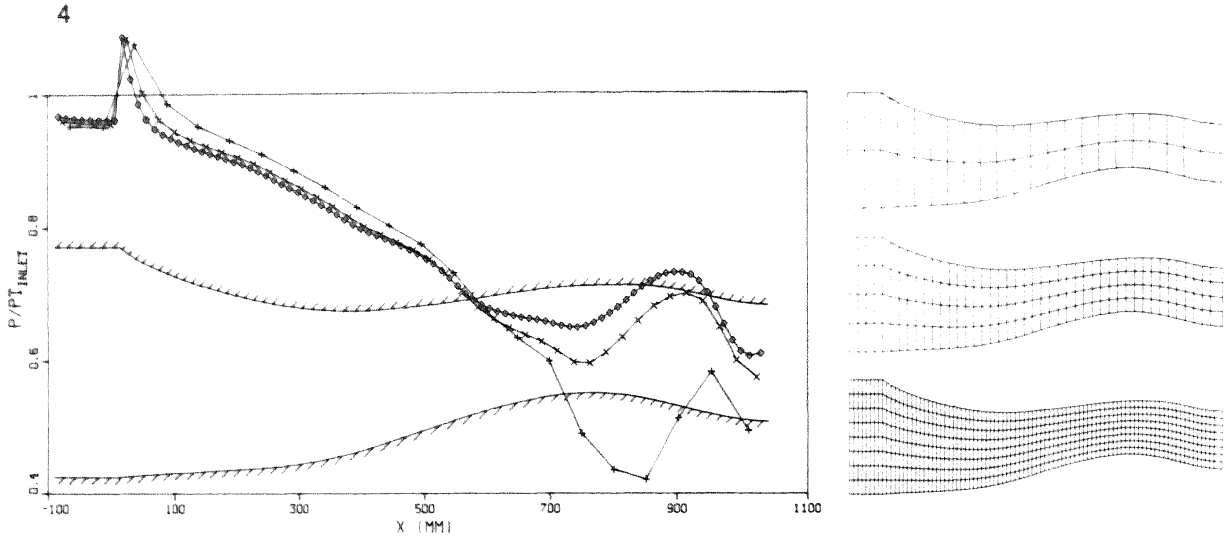

FIGURE 3.2a Pressure distribution along upper wall for a family of equidistant grids.

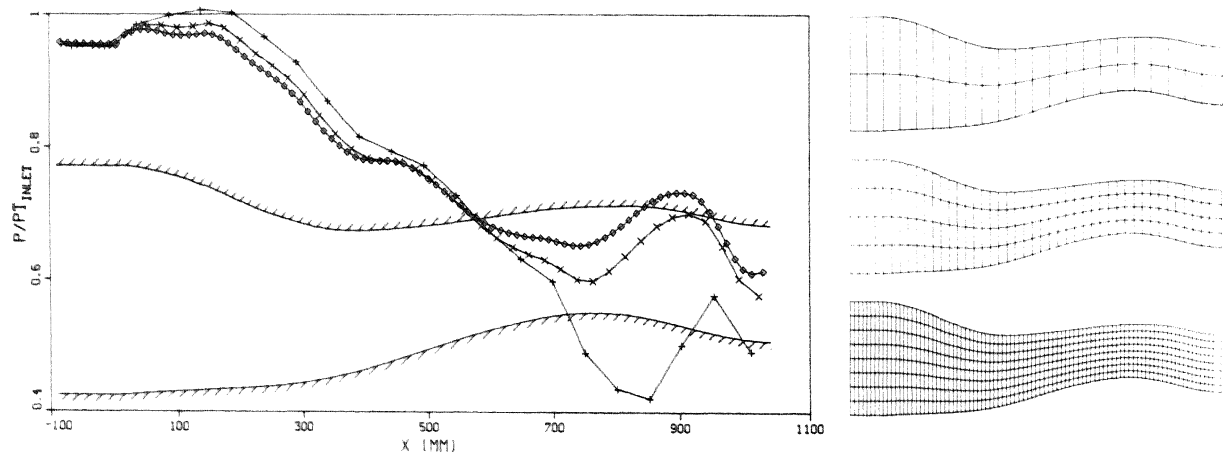

FIGURE 3.2b Pressure distribution along smoothed upper wall for a family of equidistant grids.

For the stretching of the grid the following mapping between x,y- and ξ,η-coordinates of volume vertices has been used:

$$\left.\begin{aligned} x &= x_s + (x_{\min} - x_s)\frac{e^{c_{x_1}\frac{\xi-\xi_s}{\xi_{\min}-\xi_s}} - 1}{e^{c_{x_1}} - 1} \quad ; \ \xi_{\min} \leqslant \xi \leqslant \xi_s \\ x &= x_s + (x_{\max} - x_s)\frac{e^{c_{x_2}\frac{\xi-\xi_s}{\xi_{\max}-\xi_s}} - 1}{e^{c_{x_2}} - 1} \quad ; \ \xi_s \leqslant \xi \leqslant \xi_{\max} \end{aligned}\right\}, \text{ with} \tag{3.1}$$

$$\xi = \xi_{\min} + i\Delta\xi; \ i = 0, \ldots, n_{x_1} + n_{x_2}; \ \Delta\xi = \frac{\xi_{\max} - \xi_{\min}}{n_{x_1} + n_{x_2}}, \text{ and} \tag{3.2}$$

$$\xi_{\min} = x_{\min}, \quad \xi_{\max} = x_{\max}, \quad \xi_s = \xi(i = n_{x_1}), \tag{3.3}$$

and:

$$y = y_{\min}(\xi) + (y_{\max}(\xi) - y_{\min}(\xi)) \frac{e^{c_y \frac{\eta - \eta_{\min}(\xi)}{\eta_{\max}(\xi) - \eta_{\min}(\xi)}} - 1}{e^{c_y} - 1}, \text{ with} \tag{3.4}$$

$$\eta = \eta_{\min}(\xi) + j\Delta\eta; \quad j = 0, \ldots, n_y; \quad \Delta\eta = \frac{\eta_{\max}(\xi) - \eta_{\min}(\xi)}{n_y}, \text{ and} \tag{3.5}$$

$$\eta_{\min}(\xi) = y_{\min}(\xi), \quad \eta_{\max}(\xi) = y_{\max}(\xi). \tag{3.6}$$

In these relations x and y denote the coordinates in the physical domain, and ξ and η the corresponding coordinates in the computational domain. The coordinates $x_{\min}$ and $x_{\max}$ denote the x-coordinate of the vertical grid line at the inlet and at the outlet respectively. The coordinate x_s denotes the x-coordinate of a vertical grid line which is supposed to lie in the shock wave. The functions $y_{\min}(\xi)$ and $y_{\max}(\xi)$ denote the y-coordinates of the lower and upper wall. Finally, the quantities c_{x_1}, c_{x_2}, c_y and n_{x_1}, n_{x_2}, n_y denote stretching parameters and numbers of volumes.

The y-coordinates of the lower and upper wall in the curved channel part were known from accurate measurements at discrete x-positions. In order to know the y-coordinates of lower and upper wall at arbitrary x-positions in the curved channel part, cubic spline interpolation has been used.

Smoothness requirements imposed on (3.1) and (3.4) are:

$$\frac{1}{1+\delta} \leqslant \frac{x(i+1) - x(i)}{x(i) - x(i-1)} \leqslant 1 + \delta, \quad \text{for } i = 1, \ldots, n_{x_1} + n_{x_2} - 1, \text{ and} \tag{3.7}$$

$$\frac{y(j+1) - y(j)}{y(j) - y(j-1)} \leqslant 1 + \delta, \quad \text{for } j = 1, \ldots, n_y - 1, \tag{3.8}$$

with δ some constant for limiting the stretching. Requirement (3.7) and (3.8) are approximately equal to

$$\frac{-\delta}{1+\delta} \leqslant \frac{\frac{d^2x}{d\xi^2}\Delta\xi}{\frac{dx}{d\xi}} \leqslant \delta, \quad \text{for } \xi_{\min} < \xi < \xi_{\max}, \text{ and} \tag{3.9}$$

$$\frac{\frac{d^2y}{d\eta^2}\Delta\eta}{\frac{dy}{d\eta}} \leqslant \delta, \quad \text{for } \eta_{\min}(\xi) < \eta < \eta_{\max}(\xi). \tag{3.10}$$

This gives for (3.1): $\frac{c_{x_1}}{n_{x_1}} \leqslant \frac{\delta}{1+\delta}$ and $\frac{c_{x_2}}{n_{x_2}} \leqslant \delta$, and for (3.4): $\frac{c_y}{n_y} \leqslant \delta$. So the coarsest grid imposes the strongest constraint on the stretching.

Finally, for the finest grid only, a matching requirement has been imposed. This matching requirement is

$$\frac{x(n_{x_1}+1) - x(n_{x_1})}{x(n_{x_1}) - x(n_{x_1}-1)} = 1. \tag{3.11}$$

For example, consider a 4-level multigrid strategy with for the coarsest grid: $n_{x_1} = 5, n_{x_2} = 2$ and $n_y = 1$. Taking e.g. $\delta = 1$, one obtains: $c_{x_1} \leqslant 2.5$, $c_{x_2} \leqslant 2.0$ and $c_y \leqslant 1.0$. Taking $x_s = 750$ and $c_{x_1} = 2.5$, requirement (3.11) yields (knowing $x_{\min} = -90$ and $x_{\max} = 1040$): $c_{x_2} = 2.348$. This does not satisfy $c_{x_2} \leqslant 2.0$. Iteratively lowering c_{x_1} with e.g. a factor 0.9, and determining c_{x_2} until $c_{x_2} \leqslant 2.0$ yields:

$c_{x_1} = 2.025$ and $c_{x_2} = 1.850$.

This approach has been followed for the grid generation, and the aforementioned values of n_{x_1}, n_{x_2}, n_y and δ have been chosen for all computations.

The value of x_s has not been chosen, but has been initialized to the x-location of the windtunnel throat ($x = 750$), and has been adapted to the shock location during the FMG-phase. The adaptation of x_s is motivated by the fact that the finest grid contains only 3 equidistant and most closely spaced grid lines to capture the shock. The GAMM-channel grid [4] contains about 20 of these grid lines for this purpose. Our grid adaptation is simple. First, after each solution prolongation, we search for the x-location of the maximum velocity gradient at the lower wall, downstream of the throat, and we assign this location to x_s. Hereafter, we generate the new grids. Without any correction the states q_{ij} are shifted together with the volumes Ω_{ij}. Doing this the quality of the finest grid solution as yielded by FMG becomes worse. However, no significant deterioration of convergence rates has been observed.

4. Boundary Conditions.

Boundary conditions should be correct both mathematically and physically. Mathematical theory prescribes the number of boundary conditions to be imposed. The number depends on the type of flow at a boundary. These types and the corresponding number of boundary conditions are: supersonic inflow (4), subsonic inflow (3), subsonic outflow (1), supersonic outflow (0) and impermeable walls (1).

The prescribed or expected flow behaviour is a first guideline of what specific boundary conditions to impose. For the channel flow considered some general flow properties had been prescribed. Further, use has been made of the expected flow behaviour.

Upper and lower wall: At impermeable walls, as the upper and lower wall are, the impermeability itself yields the boundary condition to be imposed: a zero normal velocity component.

Inlet: The inlet flow has been prescribed to be subsonic, so requiring 3 boundary conditions. Constant values $u = u_{inlet}, v = 0$ and either $c = c_{inlet}$ or $s = s_{inlet}$ have been chosen, with c denoting the speed of sound ($\sqrt{\gamma p / \rho}$) and s the entropy (p / ρ^{γ}). These choices were motivated by the fact that the inlet part is flat and parallel. Values for u_{inlet} and c_{inlet} have been found by using the known channel geometry and the 1-D flow theory.

Outlet: The outlet flow may be subsonic as well, so requiring 1 boundary condition. Because of the fact that the outlet part is non-flat and non-parallel, the outlet boundary condition cannot be as trivial as those at the inlet. The following possibilities have been considered:

(1.) $h = h_{inlet}$, h denoting the total enthalpy, (2.) $\frac{v}{u} = \frac{v}{u}(y)$, (3.) $u = u(y)$, and (4.) $p = p(y)$.

The first possibility was motivated by the fact that with a known uniform total enthalpy at the inlet, this boundary condition requires no knowledge of the non-uniform outlet flow. This because of the fact that for steady flows, with at the upstream boundary the total enthalpy known to be constant, only 3 differential equations describe the flow. The energy equation in its differential form may be replaced by the relation $h = \frac{1}{\gamma - 1} c^2 + \frac{1}{2}(u^2 + v^2) = h_{upstream}$ throughout the whole flow field. Although this simplifying property has not been used in the way suggested here (The code has been developed to solve the non-iso-energetic Euler equations.), it might still be used for the formulation of the outlet boundary condition.

The second possibility, with the flow direction specified, was motivated by its simplicity. A linear distribution of the flow direction has been assumed, using the known flow direction at the lower and upper wall.

The third possibility was also motivated by its simplicity. For this possibility the outlet flow has been assumed to be a potential vortex flow. The relation $ur(y) =$ constant has been applied, with $r(y)$

the distribution of the radii of curvature of the streamlines. A linear distribution for the streamline curvature $1/r(y)$ has been assumed, using the known curvature of the lower and upper wall. The constant has been determined by using the 1-D flow theory. A disadvantage of this boundary condition is its inconsistency in the case of a flow with shock wave. It is a boundary condition which is always consistent in a potential flow model, but not in the Eulerian rotational flow model.

The fourth possibility was motivated by the good flow tuning it allows, as known from previous computations. For this possibility the equation of curvilinear motion

$$\frac{dp(y)}{dy} = \gamma \frac{p(y)M^2(y)}{r(y)} \cos(\theta(y)) \tag{4.1}$$

has been used, with $M(y)$ the Mach number distribution and $\theta(y)$ the distribution of the angles between the streamlines and the x-axis. $M(y)$ has been taken constant. Its value has been determined with the 1-D flow theory. For $1/r(y)$ and $\theta(y)$, again linear distributions have been used, such that the flow fits the channel outlet. Using a 1-D flow theory value of p as value for p at the lower wall, an initial value problem is obtained. The initial value problem has been solved numerically. For this a Runge-Kutta-Merson method could be used.

A mathematically well-posed boundary condition is a boundary condition for which the state at the boundary can be determined accurately. The outlet boundary condition should determine 1 degree of freedom, and hence it can be seen as a 3-D surface in the 4-D state space. The smaller the angle α between the normal at this surface and the eigenvector corresponding with the negative eigenvalue $(u-c)$, the better the quality of the boundary condition. Considering the (ρ,u,v,e)-space as state space, the eigenvector corresponding with the eigenvalue $u-c$ is: $r = (\rho, -c, 0, c(\frac{1}{\gamma}c - u))$. For respectively h, v/u, u or p specified, the 3-D surface is described by

$$B(q) = \gamma e - \frac{\gamma-1}{2}(u^2 + v^2) = h_{outlet}, \tag{4.2a}$$

$$B(q) = \frac{v}{u} = (\frac{v}{u})_{outlet}, \tag{4.2b}$$

$$B(q) = u = u_{outlet}, \text{ and} \tag{4.2c}$$

$$B(q) = (\gamma - 1)\rho(e - \tfrac{1}{2}(u^2 + v^2) = p_{outlet}. \tag{4.2d}$$

The angle α is determined by $\cos(\alpha) = \dfrac{\nabla B \cdot r}{\|\nabla B\| \, \|r\|}$, with $\nabla B = (\dfrac{\partial B}{\partial \rho}, \dfrac{\partial B}{\partial u}, \dfrac{\partial B}{\partial v}, \dfrac{\partial B}{\partial e})$. For respectively $h,v/u,u$ or p specified, we find

$$\nabla B \cdot r = c(u-c), \tag{4.3a}$$

$$\nabla B \cdot r = \frac{v}{u}\frac{c}{u}, \tag{4.3b}$$

$$\nabla B \cdot r = -c, \tag{4.3c}$$

$$\nabla B \cdot r = \frac{1}{\gamma - 1}p. \tag{4.3d}$$

From (4.3a) and (4.3b) it can be seen that for h or v/u specified, the vectors ∇B and r may become orthogonal for $u \to c$ respectively $v \to 0$. Consider for instance the state at the outlet to be: $(\rho,u,v,c) = (1.0, 0.75, -0.1, 1.0)$. For this particular state we find: $\cos(\alpha) = 0.123$ (h specified), $\cos(\alpha) = -0.070$ (v/u specified), $\cos(\alpha) = -0.707$ (u specified) and $\cos(\alpha) = 0.810$ (p specified).

The consequence of a nearly orthogonal ∇B and r is that a small change in either the boundary condition or the state in the domain, near the outlet, may cause a large change in the boundary state and hence in the flux across the boundary. For a given state $q_0 = (u_0, v_0, c_0, z_0)$ near the outlet, and

the boundary conditions specified by (4.2a) - (4.2d) respectively, the effect of a perturbation in q_0 will be shown. The state at the boundary is $q = (u, v_0, c, z_0)$, with

$$\left.\begin{aligned} c &= \frac{\gamma-1}{\gamma+1}\{u_0 + \frac{2}{\gamma-1}c_0 + \sqrt{(\gamma+1)(h_{outlet} - \tfrac{1}{2}v_0^2) - \frac{\gamma-1}{2}(u_0 + \frac{2}{\gamma-1}c_0)^2}\} \\ u &= u_0 + \frac{2}{\gamma-1}(c_0 - c) \end{aligned}\right\}, \tag{4.4a}$$

$$\left.\begin{aligned} u &= \frac{v_0}{(\frac{v}{u})_{outlet}} \\ c &= c_0 + \frac{\gamma-1}{2}(u_0 - u) \end{aligned}\right\}, \tag{4.4b}$$

$$\left.\begin{aligned} u &= u_{outlet} \\ c &= c_0 + \frac{\gamma-1}{2}(u_0 - u) \end{aligned}\right\}, \text{ and} \tag{4.4c}$$

$$\left.\begin{aligned} c &= \sqrt{\gamma_{p_{outlet}}^{\frac{\gamma-1}{\gamma}} e^{\frac{z_0}{\gamma}}} \\ u &= u_0 + \frac{2}{\gamma+1}(c_0 - c) \end{aligned}\right\}, \tag{4.4d}$$

for the boundary conditions (4.2a) - (4.2d) respectively. The corresponding gradients $\nabla u = (\frac{\partial u}{\partial u_0}, \frac{\partial u}{\partial v_0}, \frac{\partial u}{\partial c_0}, \frac{\partial u}{\partial z_0})$ and $\nabla c = (\frac{\partial c}{\partial u_0}, \frac{\partial c}{\partial v_0}, \frac{\partial c}{\partial c_0}, \frac{\partial c}{\partial z_0})$ are

$$\left.\begin{aligned} \nabla c &= \frac{\gamma-1}{\gamma+1}\{(1, 0, \frac{2}{\gamma+1}, 0) - \frac{1}{c-u}(\frac{\gamma-1}{2}u + c, \frac{\gamma+1}{2}v, u + \frac{2}{\gamma-1}c, 0)\} \\ \nabla u &= (1, 0, \frac{2}{\gamma-1}, 0) - \frac{2}{\gamma-1}\nabla c \end{aligned}\right\}, \tag{4.5a}$$

$$\left.\begin{aligned} \nabla u &= (0, \frac{u}{v}, 0, 0) \\ \nabla c &= (\frac{\gamma-1}{2}, -\frac{\gamma-1}{2}\frac{u}{v}, 1, 0) \end{aligned}\right\}, \tag{4.5b}$$

$$\left.\begin{aligned} \nabla u &= 0 \\ \nabla c &= (\frac{\gamma-1}{2}, 0, 1, 0) \end{aligned}\right\}, \text{ and} \tag{4.5c}$$

$$\left.\begin{aligned} \nabla c &= (0, 0, 0, \frac{1}{2\gamma}c) \\ \nabla u &= (1, 0, \frac{2}{\gamma-1}, \frac{-1}{\gamma(\gamma-1)}c) \end{aligned}\right\}, \tag{4.5d}$$

where we took $q = q_0$ in (4.4a) for simplicity. It can be seen that the gradient pairs (4.5a) and (4.5b) may become infinitely large in aforementioned limit cases ($u \to c$ for h specified and $v \to 0$ for v/u specified). Flow computations with h specified and v/u specified showed these outlet boundary conditions to be ill-posed indeed. This was not the case with the two other boundary conditions.

Because of its better consistency, the boundary condition with p specified has been used for the flow solutions shown in the next section.

5. Results

For the transonic channel flow proposed in [4], very good convergence rates were obtained with the present code by using only a very simple multigrid strategy (V-cycles with only 1 symmetrical pre- and post-relaxation at each grid.) For the transonic flow in the present channel a bad convergence rate was obtained (or no convergence at all), when the same multigrid strategy was used.

In each volume of the coarsest grid (7×1), the progress of the Newton iteration was studied during several relaxation sweeps. It appeared that in all volumes after one or two Newton steps the iteration converged quadratically and continued to convergence in this way. However, it appeared that once the Euler solution in a volume had been obtained, the residual in the next volume had been strongly increased. In the evolution of the volume residuals during many relaxation sweeps one could observe a very slowly but nevertheless continuously decreasing overall residual. The evolution of the solution during many relaxation sweeps showed the slowly vanishing error to be a low frequency error component. Relaxation sweeps on an even coarser grid (4×1) showed the same behaviour. It was not until a 2×1-grid that a good convergence rate was obtained. From this it could be concluded that when retaining point Gauss-Seidel (for its simplicity) and a 7×1 coarsest grid, the number of relaxations at the coarsest grid should be taken much higher (10 to 15 symmetrical pre- and post-relaxations instead of 1).

Multigrid computations with many relaxations on the coarsest grid, showed that only 1 symmetrical pre- and post-relaxation on the finer grids was insufficient as well. An experiment for a 112×16 finest grid, with V-cycles with 15 symmetrical pre- and post-relaxations at the coarsest grid and 3 symmetrical pre- and post-relaxations at the finer grids has been performed. For this experiment, in figure 5.1 a norm of the finest grid residual after each pre- and post-relaxation has been given. The norm used is the largest value of the L_1-norm of the 4 components in the residual.

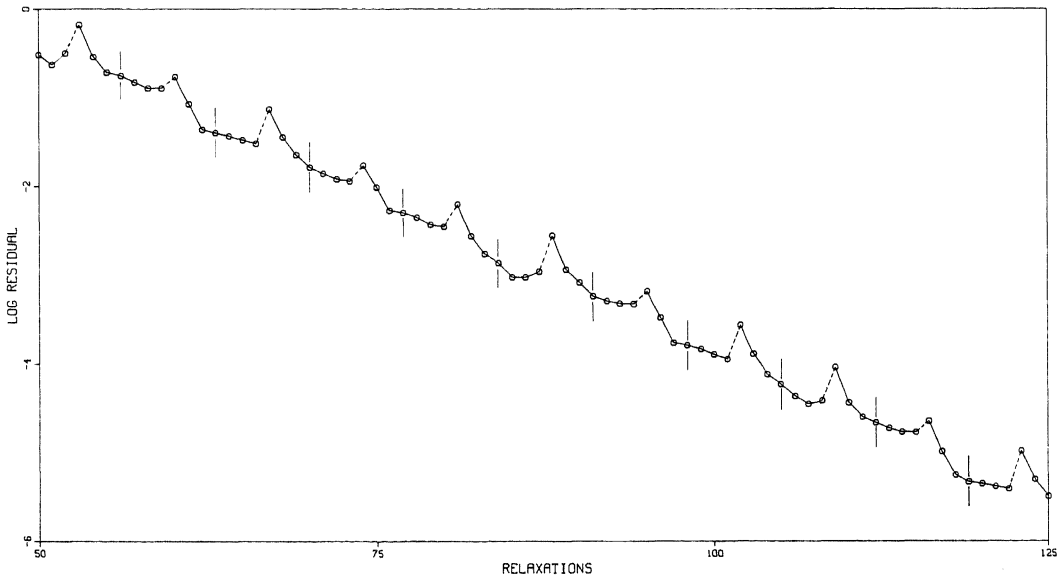

FIGURE 5.1 Convergence history for experimental multigrid strategy.

The vertical lines indicate the beginnings and ends of the FAS-cycles, and the dashed parts represent the coarse grid corrections. From figure 5.1 it appears that multigrid starts to work when more than 1 post-relaxation at the finest grid is used. As fixed multigrid strategy for the computations we have chosen: V-cycles with symmetrical pre- and post-relaxations; 15 pre- and post-relaxations at the coarsest grid and 1 pre-relaxation and 3 post-relaxations at the finer grids.

Computational results obtained for a choked respectively a non-choked flow are shown in figure 5.2a - 5.2f and figure 5.3a - 5.3f. Again, the markers in fig. 5.2b, 5.2c, 5.3b and 5.3c indicate the x-locations of the centres of the volume walls.

In figure 5.2a and 5.3a the finest grids obtained are given. Comparing figure 5.2a and 5.2b, and figure 5.3a and 5.3b it can be seen that for both flows the grid adaptation is good. Both figure pairs show the shock wave to be captured in the finest volumes.

Comparing figure 5.2b and 5.2c, and figure 5.3b and 5.3c, it can be seen that the ratios across the shock wave of M, p and s, agree with the Mach number just in front of the shock wave. Furthermore, the shock wave is sharp.

The entropy distributions in figure 5.2c and 5.3c show a slight monotone increase in downstream direction. This inaccuracy is generally found for Euler codes (entropy error). Remarkable in both figures is that the entropy rise in the supersonic region is stronger than that in the subsonic region. A good explanation of this feature is still lacking. Reduction of the entropy error can be obtained by increasing the order of accuracy of the discretization.

Clearly visible in both figure 5.2b and 5.3b is the occurrence of an after-expansion. Since the Osher scheme yields monotone solutions for first order accurate up- and downwind states, the after-expansion occurring in both flows is not a numerical artefact but a correct part of the Euler flow solutions indeed.

Finally, in both figure 5.2b and 5.3b the coincidence is visible of the intersections of the lower and upper wall pressure curves with the (approximately coinciding) inflexion points in lower and upper wall. This coincidence is in agreement with the equation of curvilinear motion.

6. Conclusions

For the windtunnel section described in [1], monotone solutions with sharp shocks have been obtained with the method described in [2]. Further, the overall quality of the solutions seems to be good.

The adaptation of the grid to the shock position during the FMG-phase works well. In almost all cases considered, the shock was captured in the two finest volumes.

An outlet boundary condition with total enthalpy or flow direction specified yields a mathematically ill-posed problem, whereas an outlet boundary condition with static pressure specified yields a mathematically well-posed problem.

The convergence rates obtained for the present channel are not as good as those obtained (with the present code) for the GAMM-channel [4]. The convergence rates can be improved by using e.g. line relaxation with lines in streamwise direction.

Acknowledgements

The authour would like to thank P.W. Hemker, S.P. Spekreijse and P.M. de Zeeuw for their valuable suggestions, and P.M. Zeeuw furthermore for his spline fitting software.

This work was supported by the Netherlands Technology Foundation (STW).

7. REFERENCES.

[1] NEBBELING, C., BANNINK, W.J., *"A curved test section for research on transonic shock wave-boundary layer interaction."* Report LR-414, Delft University of Technology, 1984.

[2] HEMKER, P.W., SPEKREIJSE, S.P., *"Multiple grid and Osher's scheme for the efficient solution of the steady Euler equations."* Report NM-R8507, Centre for Mathematics and Computer Science, Amsterdam, 1985.

[3] OSHER, S., *"Numerical solution of singular perturbation problems and hyperbolic systems of conservation laws."* In: Mathematical and numerical approaches to asymptotic problems in analysis. Axelsson, O., Frank, L.S. and van der Sluis, A. (eds.), North-Holland Publishing Company, 1981.

[4] RIZZI, A., VIVIAND, H., *"Numerical methods for the computation of inviscid transonic flows with shock waves."* Proceedings GAMM Workshop, Stockholm, 1979, Vieweg Verlag, 1981.

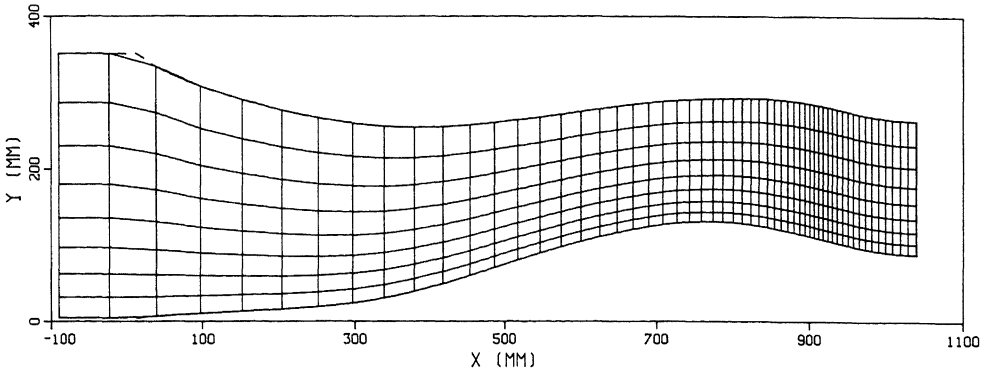

FIGURE 5.2a Finest grid obtained.

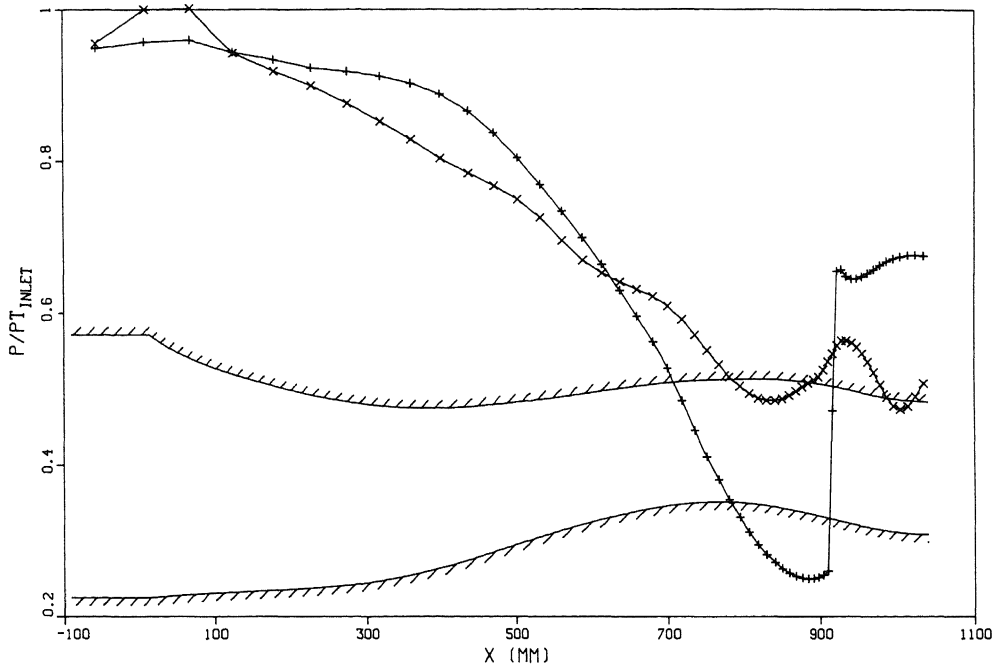

FIGURE 5.2b Pressure distribution along lower and upper wall.

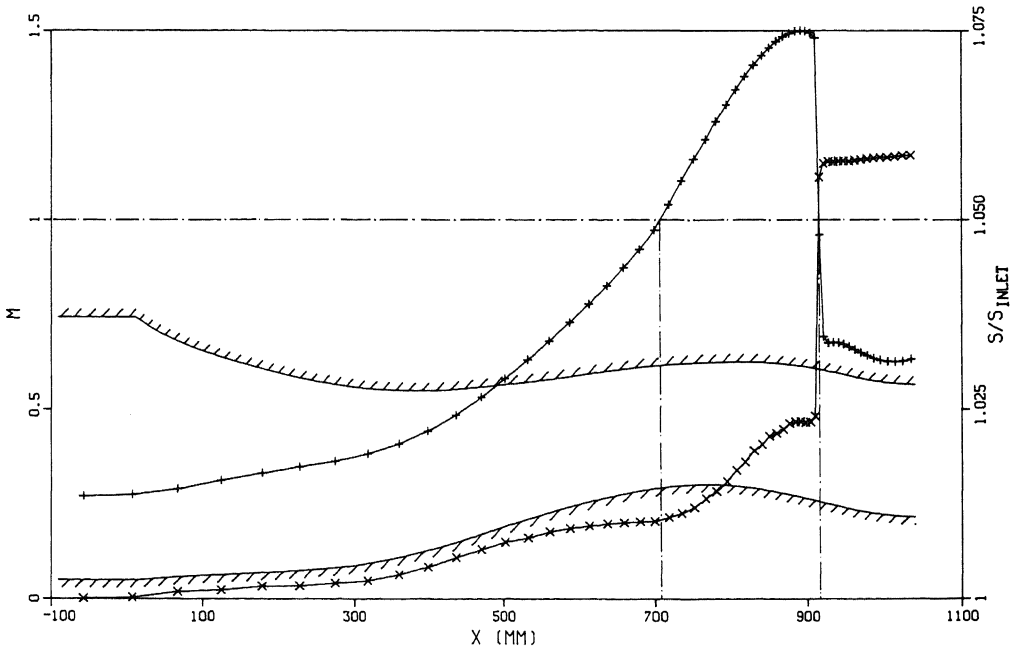

FIGURE 5.2c Mach number and entropy distribution along lower wall.

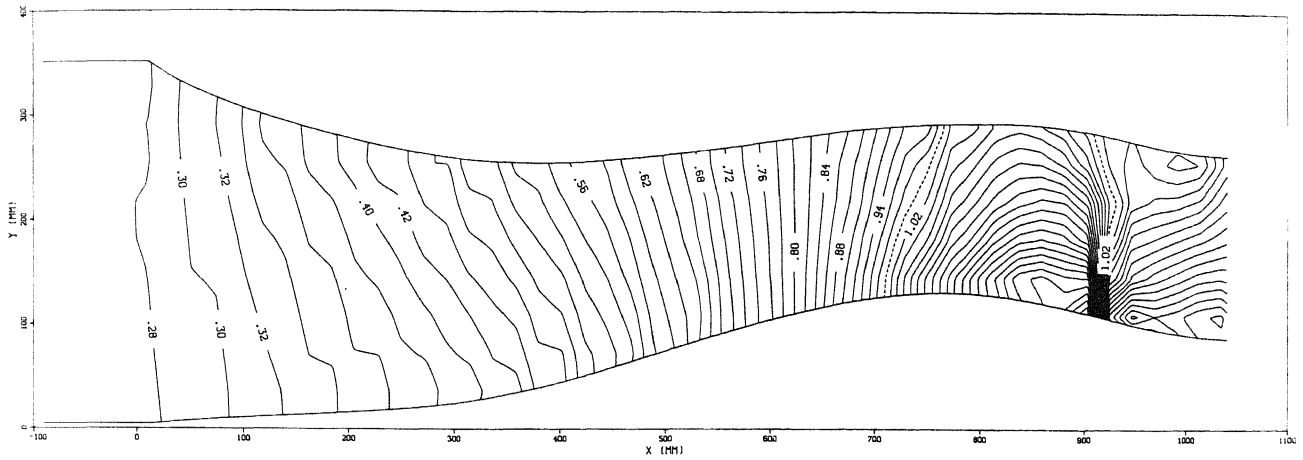

FIGURE 5.2d Mach number distribution.

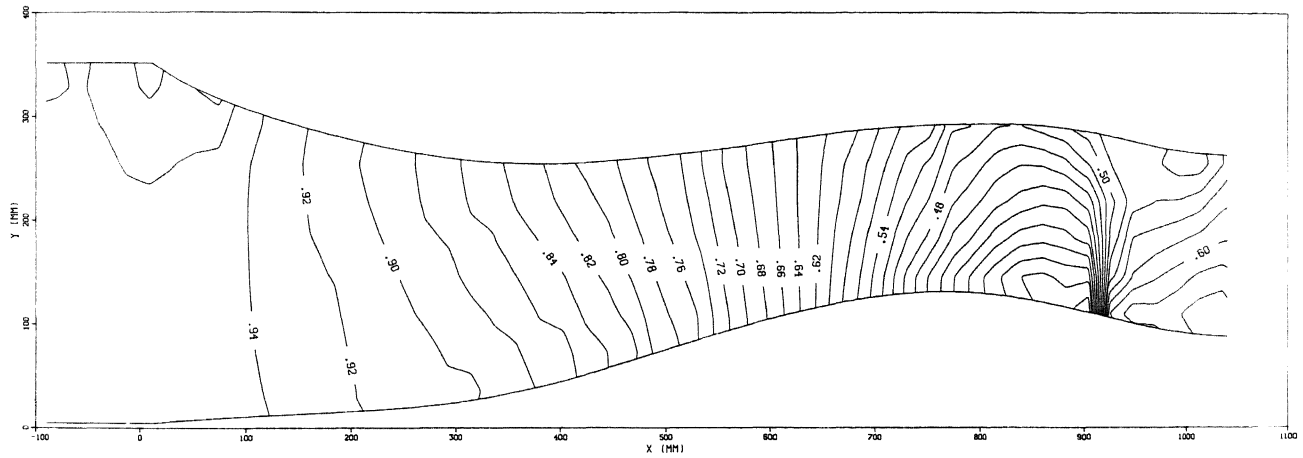

FIGURE 5.2e Pressure distribution ($p / p_{t_{inlet}}$).

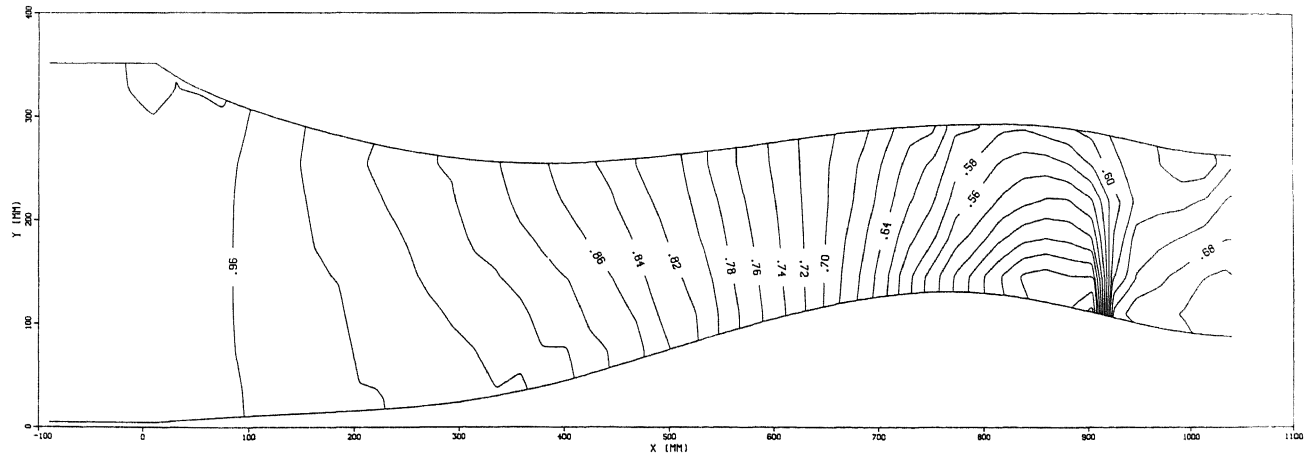

FIGURE 5.2f Density distribution ($\rho / \rho_{t_{inlet}}$).

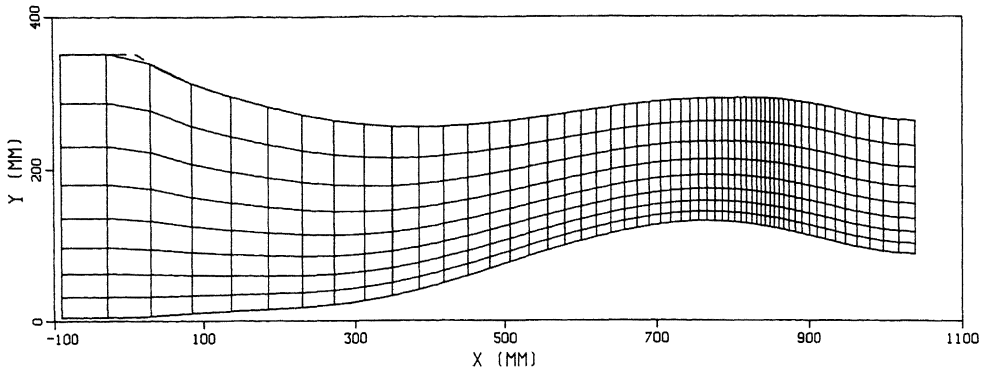

FIGURE 5.3a Finest grid obtained.

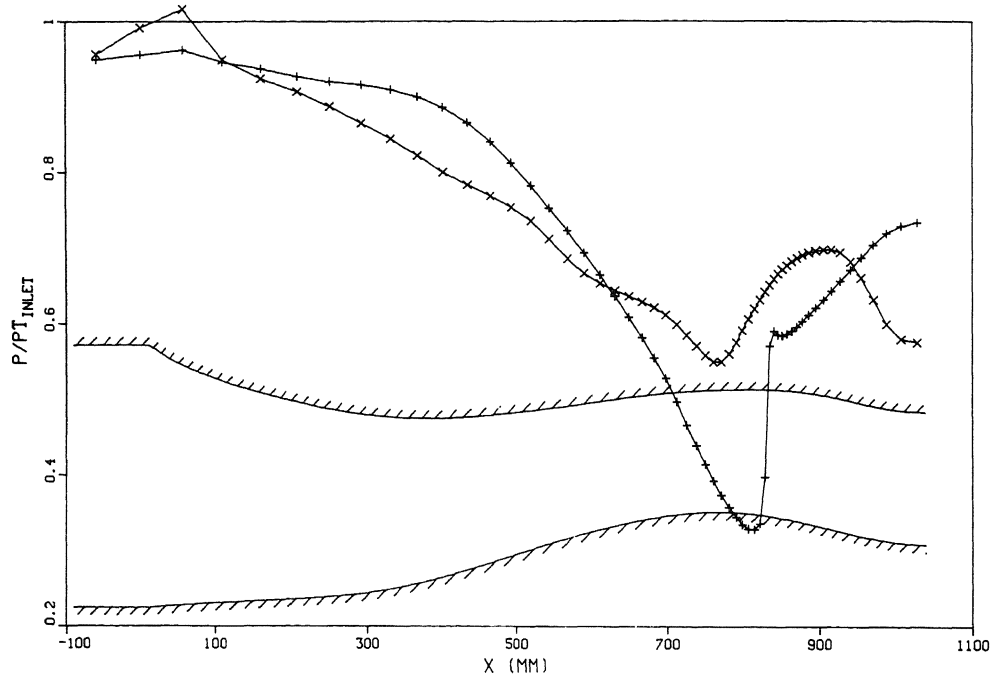

FIGURE 5.3b Pressure distribution along lower and upper wall.

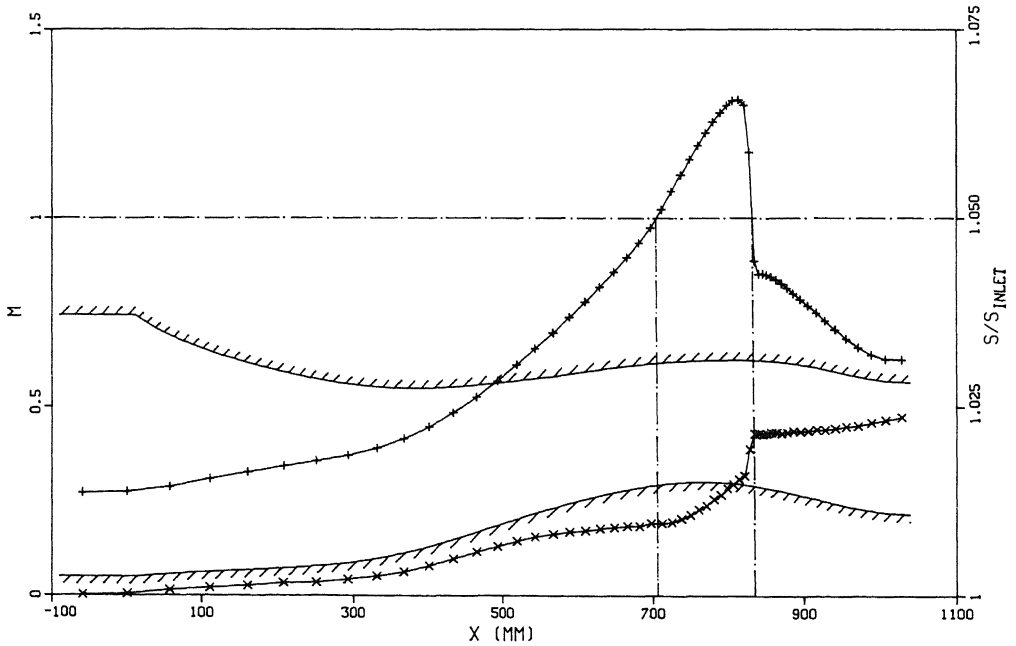

FIGURE 5.3c Mach number and entropy distribution along lower wall.

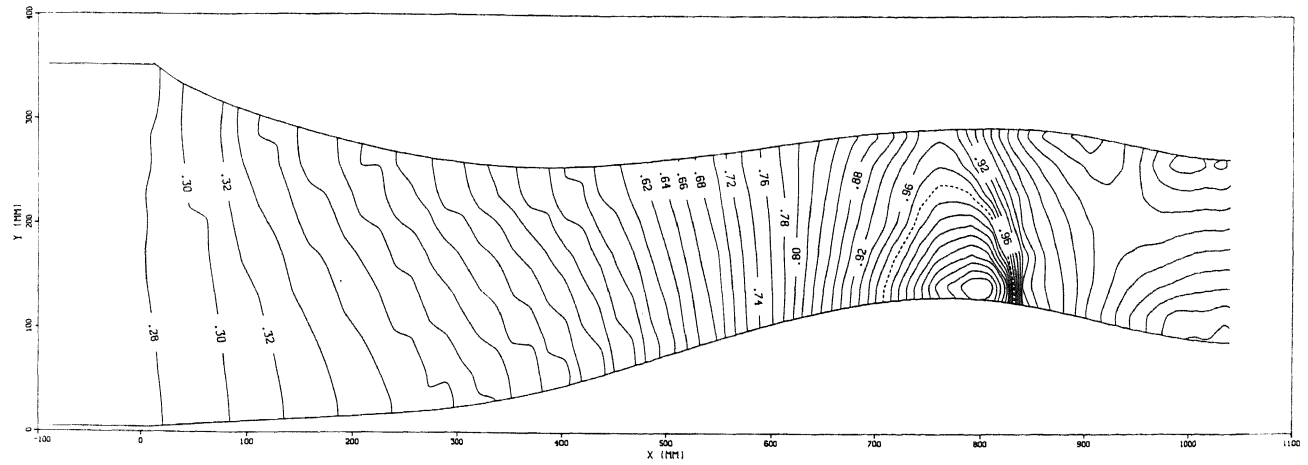

FIGURE 5.3d Mach number distribution.

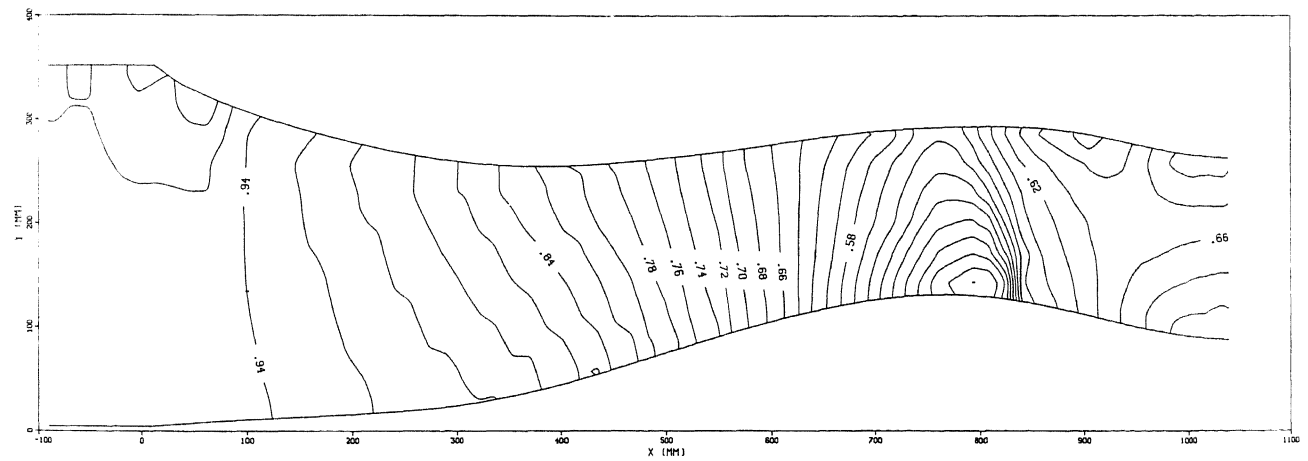

FIGURE 5.3e Pressure distribution ($p / p_{t_{inlet}}$).

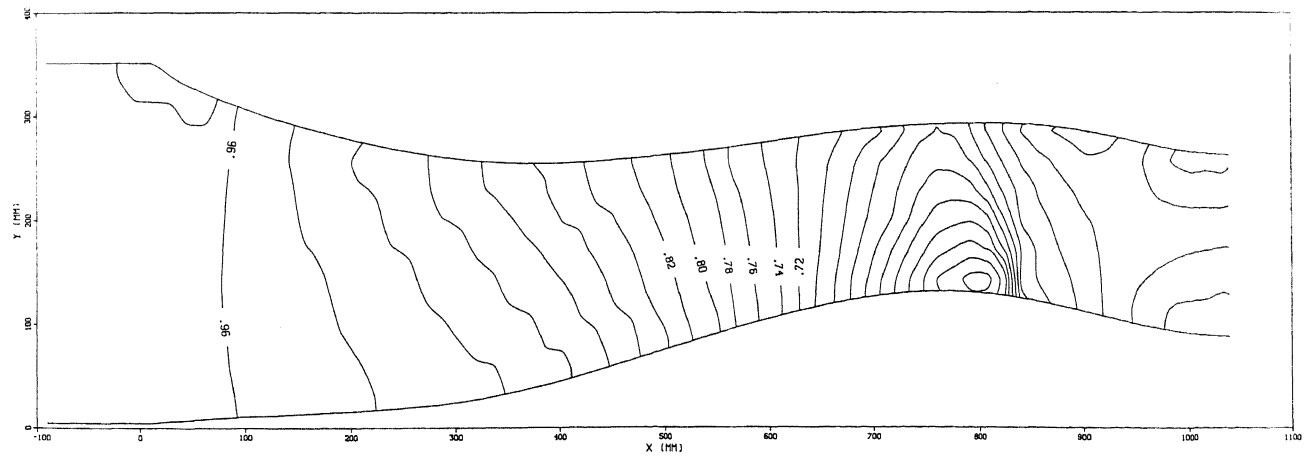

FIGURE 5.3f Density distribution ($\rho / \rho_{t_{inlet}}$).